

15.7 ANALYSIS OF THE EVOLUTION OF AN URBAN BOUNDARY LAYER AS DETECTED BY A FREQUENCY MODULATED-CONTINUOUS WAVE RADAR

Frank W. Gallagher III^{1*}, James F. Bowers¹, Eric J. Laufenberg¹, Edward P. Argenta Jr.¹, Donald P. Storwold¹, and Scott A. McLaughlin²

¹West Desert Test Center, U.S. Army Dugway Proving Ground, Dugway, UT

²Applied Technologies, Inc., Longmont, CO

1. Introduction

Frequency modulated-continuous wave (FM/CW) radars have been used for a number of years to investigate the evolution of the boundary layer (e.g. Metcalf, 1975; Eaton et al., 1995; Dekker et al., 2002; Heijnen et al., 2003; Ince et al., 2003). Typically, the radars are positioned in rural environments as part of larger experiments. During the summer of 2003, the West Desert Test Center deployed an S-band (2.9 GHz) FM/CW radar just north of the central business district of Oklahoma City, OK in support of the Joint Urban 2003 urban dispersion experiment (Allwine et al., 2004). The primary objective was to observe the normal diurnal cycle of the urban boundary layer. However, the radar observed several unusual aspects of the urban convective boundary layer that made assigning a single boundary layer height difficult.

2. The Army FM/CW Atmospheric Radar

Figure 1 shows the U.S. Army Dugway Proving Ground (DPG) FM/CW atmospheric radar, which is described in more detail by McLaughlin (2003). The radar is mounted on two trailers: one trailer houses the radar electronics, while the steerable 10-foot bistatic dishes are mounted on the other. The amplifier is a 200 W traveling wave tube with a sweep time of 50 ms.

The radar is normally used to measure the vertical profile of the refractive index structure parameter, C_n^2 , with a spatial resolution of 0.5 to 10 m, depending on the detection range. Although Eaton et al. (1988) show a direct relationship between the received power, radar system parameters, and C_n^2 , the C_n^2 values measured by the Dugway FM/CW during Joint Urban 2003 were relative rather than absolute. The radar equation was used to process the received signal, and non-linear terms of the radar equation were applied. An absolute calibration for C_n^2 , which was not performed, would have involved adjusting the radar equation linear quantities (e.g. hardware and processing gain). Because of ground clutter and the separation of the nearly vertically pointing (4° off vertical – to allow rain to run off the radomes) transmit and receive antennas, the lowest usable range gate is approximately 65 m.



Figure 1 – The DPG FM-CW Radar located in Oklahoma City for the Joint Urban 2003 Urban Dispersion Experiment. Also shown are the DPG SODAR (left, in front of the electronics trailer) and the Lawrence Livermore National Laboratory ceilometer.

The high spatial (3 m for this experiment) and temporal (30 s) resolution of the FM/CW radar measurements result in C_n^2 time-height cross-sections that allow one to visualize many boundary layer processes, hydrometeors, and point targets such as insects and birds. C_n^2 is an ensemble average of the square of the spatial differences in the index of refraction (at the transmit frequency) and can be written as (Vaucher and Raby, 2002)

$$C_n^2 = \frac{\langle (n_2 - n_1)^2 \rangle}{r^{2/3}} \quad (1)$$

where r is the distance between n_1 and n_2 and $n_1 = n(r_1)$ and $n_2 = n(r_2)$ are the atmospheric index of refraction at points r_1 and r_2 , respectively. C_n^2 values are high where the differences between the refractive indices of nearby points are large. Large values of C_n^2 represent a measure of high turbulence in the inertial subrange of the atmosphere. The relationship between C_n^2 and temperature and humidity fluctuations can be written as (Hill et al., 1980)

$$C_n^2 = \frac{A_T^2 C_T^2}{\langle T \rangle^2} + \frac{A_Q^2 C_Q^2}{\langle Q \rangle^2} + 2 \frac{A_T A_Q C_{TQ}}{\langle T \rangle \langle Q \rangle} \quad (2)$$

*Corresponding author address: Frank Gallagher, U.S. Army Dugway Proving Ground, Dugway, UT, 84022; e-mail: gallagf@dpq.army.mil.

where C_T^2 and C_Q^2 are respectively the temperature and humidity structure parameters, C_{TQ} is the temperature-humidity cross-structure parameter, and the brackets indicate a time average. Equation (2) is applicable to the real part of the refractive index; the coefficients A_T and A_Q vary with frequency.

As shown by Equation (2), large values of C_n^2 are associated with large values of C_T^2 and/or C_Q^2 (unless the C_{TQ} term is large and negative). Tartarskii (1971) has shown that C_T^2 is proportional to the square of the vertical potential temperature gradient. Thus, in a convective boundary layer C_T^2 (and hence C_n^2) can be expected to be large in the super-adiabatic layer near the surface and small in the well-mixed portion of the boundary layer, with high values again occurring in the elevated inversion layer at the top of the mixed layer.

3. Boundary Layer Examples

Our analysis of the evolution of the urban boundary layer over Oklahoma City began with the hypothesis that the top of the daytime boundary layer could be identified by an elevated layer of enhanced C_n^2 . As shown by several examples in this section, the FM/CW radar measurements indicate that the instantaneous structure of the daytime boundary layer can be far more complicated than this simple conceptual model. Because urban heat island and roughness effects generally can be expected to prevent the development of strong surface-based inversions downwind of the central business district, we hypothesized that the top of the nighttime boundary layer could also often be identified by an elevated layer of enhanced C_n^2 . However, little data were available to test this hypothesis because apparent point targets (possibly insects) usually appeared shortly (within an hour) after sunset in such concentrations that they obscured the meteorological signal until near sunrise.

Figure 2 shows a 1-hour record of FM/CW radar observations during a typical summertime convective day. The measurements were recorded from 1800 to 1900 UTC on 7 July 2003. At approximately 1500 m, the top of the boundary layer is clearly delineated by the stronger radar return signal denoted by the yellow, red, and white colors. Figure 3 shows the estimated boundary layer height derived from the FM/CW imagery data and an associated FFT frequency spectrum for the boundary layer wave structure between 1804 and 1814 UTC. The imagery and the corresponding derived boundary layer heights are similar to those found by Noonkester (1974) to be caused by free convection. The spectrum indicates approximately one convective updraft every 90 seconds. A similar analysis for the entire hour (not shown) shows that the oscillation frequency at the top of the boundary layer is remarkably constant (~ 0.011 Hz) throughout the hour, indicating fairly constant wind speeds and insolation. The boundary layer height and wave structure frequency remain nearly constant for the next several hours (not shown) until clouds and evaporative cooling from virga interrupt the daytime heating of the surface.

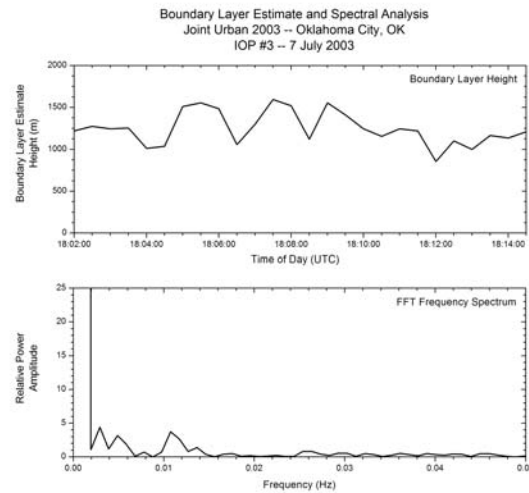


Figure 3 – Estimated boundary layer height derived from the FM/CW imagery data and a FFT frequency spectrum for the boundary layer wave structure between 1804 and 1814 UTC. The estimated height of the boundary layer was made at 30 s intervals. The relative peak in the spectrum at 0.011 Hz indicates a convective plume rate of one every 91 s.

Figures 4-6 show a 3-hour time sequence of the evolution of a daytime boundary layer from 1800 to 2100 UTC on 26 July 2003. On this day, the boundary layer develops in typical fashion (Fig. 4), although the wavelength of the boundary layer oscillation is nearly double that of the previous example. Also, a secondary residual layer of enhanced C_n^2 can be seen above the apparent top of the boundary layer. As the afternoon progresses, the periodicity of the wave structure of the top of the boundary layer begins to break down. Between 1845 and 1850 UTC, the C_n^2 profile suggests a possible overturning of the top of the boundary layer. Figures 5 and 6 show that the boundary layer depth continues to increase until it reaches a maximum height of approximately 3300 m at 2010 UTC. At this point, there appears to be a “super convective plume” that temporarily elevates the boundary layer to its maximum height of the day and causes very high C_n^2 values. After this vertical surge, the boundary layer depth appears to collapse below 1000 m (at 2020 UTC) before recovering to near the pre-super-plume height.

The C_n^2 time-height cross-sections in Figures 4-6 support the concept that the boundary layer top is highly chaotic with, at times, strong upward and downward vertical motions. Furthermore, the imagery indicates that the top of the boundary layer can overturn and, for periods of time, multiple layers of enhanced C_n^2 can be seen. For example, after the super plume event (2030 UTC), three layers of enhanced C_n^2 are evident in Figure 6. The lowest layer, at 1500 m, is probably what would be classified as the top of the convective boundary layer (CBL). The other layers of enhanced C_n^2 are at 2500 and nearly 3000 m. Even as surface heating causes the boundary layer depth to increase, the strongest of the elevated layers of enhanced C_n^2

remain above the conventional CBL top and get “pushed higher” by the increasing height of the convective boundary layer. To underscore this linkage, consider the boundary layer evolution from 2045 to 2100 UTC. The highest layer of enhanced C_n^2 shows an undulating pattern that is in concert with the growth of the CBL below.

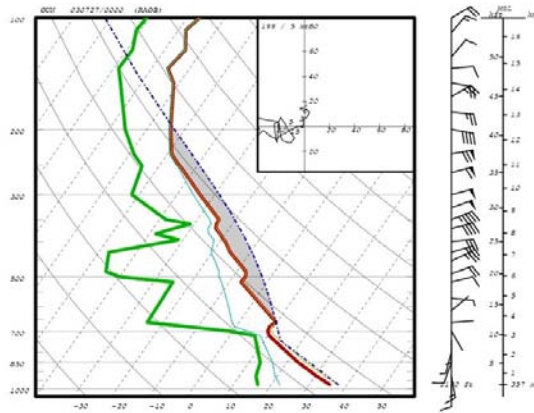


Figure 8 – Norman, OK sounding for 0000 UTC on 27 July 2003. This sounding corresponds in time with the data shown in Figure 6.

Figure 7, a time series of the vertical profile of C_n^2 recorded 3 hours later than the image in Figure 6, probably shows the demise of the CBL. Although the top of the boundary layer loses its radar signature by about 0035 UTC, elevated layers of enhanced C_n^2 remain near 3000 m. The Norman, OK 0000 UTC upper-air sounding (Fig. 8) reveals an elevated inversion above 3200 m. Not only does the lapse rate change, but also the winds shift from southerly to easterly. This inversion most likely causes the enhanced layer of C_n^2 detected by the radar.

4. Conclusions

The primary objective of the FM/CW radar measurements during Joint Urban 2003 was to observe the diurnal cycle of the urban boundary layer. The nighttime boundary layer depth usually was difficult or impossible to assign because of the lack of a clear C_n^2 signal at the top of the boundary layer and/or point targets (possibly insects) that obscured the meteorological signal. The daytime measurements revealed that the near-instantaneous structure of the boundary layer is far more complex than the simple conceptual model of a mixed layer capped by an elevated stable layer. Convective updrafts and downdrafts were evident at the top of the boundary layer, and the boundary layer depth on occasion varied rapidly over a matter of minutes.

5. Acknowledgments

The authors wish to thank the Defense Threat Reduction Agency for supporting this research.

6. References

Allwine, K.J., M.J. Leach, L.W. Stockham, J.S. Shinn, R.P. Hosker, J.F. Bowers, and J.C. Pace, 2004: Overview of Joint Urban 2003 – An atmospheric dispersion study in Oklahoma City. *8th Symposium on Integrated Observing and Assimilation Systems for Atmospheres, Oceans, and Land Surface*, Paper J7.1, American Meteorological Society, Boston, MA.

Dekker P.L., A.N. Bajaj, and S.F. Frasier, 2002: Radar and acoustic observations during VTMX field-campaign. *10th Conference on Mountain Meteorology*, Paper P1.6, American Meteorological Society, Boston, MA.

Eaton, F.D., W.A. Peterson, J.R. Hines, K.R. Peterman, R.E. Good, R.R. Beland, and J.H. Brown, 1988: Comparisons of VHF radar, optical, and temperature fluctuation measurements of C_n^2 , τ_0 , and θ_0 . *Theor. Appl. Climatol.*, **39**, 17-29.

Eaton, F.D., S.A. McLaughlin, and J.R. Hines, 1995: A new frequency-modulated continuous wave radar for studying planetary boundary layer morphology. *Radio Sci.*, **30**, 75-88.

Heijnen, S.H., H. Klein-Baltink, H.W.J. Russchenberg, H. Verlinde, and W.F. van der Zwan, 2002: Boundary layer measurements with a 3 GHz FMCW atmospheric profiler. *15th Conference on Boundary Layer and Turbulence*, Paper 7.8, American Meteorological Society, Boston, MA.

Ince, T., S.J. Frasier, A. Muschinski, and A.L. Pazmany, 2003: An S-band frequency-modulated continuous-wave boundary layer profiler: Description and initial results. *Radio Sci.*, **38**, 1072

Hill, R.J., S.F. Clifford, and R.S. Lawrence, 1980: Refractive-index and absorption fluctuations in the infrared caused by temperature, humidity, and pressure fluctuations. *J. Opt. Soc. Am.*, **70**, 1192-1204.

McLaughlin, S.A., 2003: A new data acquisition system for the U.S. Army FM-CW radar: Still a great way to see half-meter resolution. *12th Symposium on Meteorological Observations and Instrumentation*, Paper P1.20, American Meteorological Society, Boston, MA.

Metcalf, J.I., 1975: Microstructure of radar echo layers in the clear atmosphere. *J. Atmos. Sci.*, **32**, 362-370.

Noonkester, V.R., 1974: Convective activity observed by FM-CW radar. Naval Electronics Lab. Center, NELC/TR 1919. San Diego, CA 92152, 70 pp.

Tatarskii, V.I., 1971: *The Effects of the Turbulent Atmosphere on Wave Propagation (English Translation)*. J.W. Strohbehn (ed.), Israel Program for Scientific Translation, Jerusalem. Available from NTIS, Springfield, VA.

Vaucher, G.-T., and J. Raby, 2002: Exploiting environmental conditions: atmospheric stability transition forecasting. *Proceedings of the Army Science Conference (ASC'02)*, Orlando, FL, Dec. 2-5.

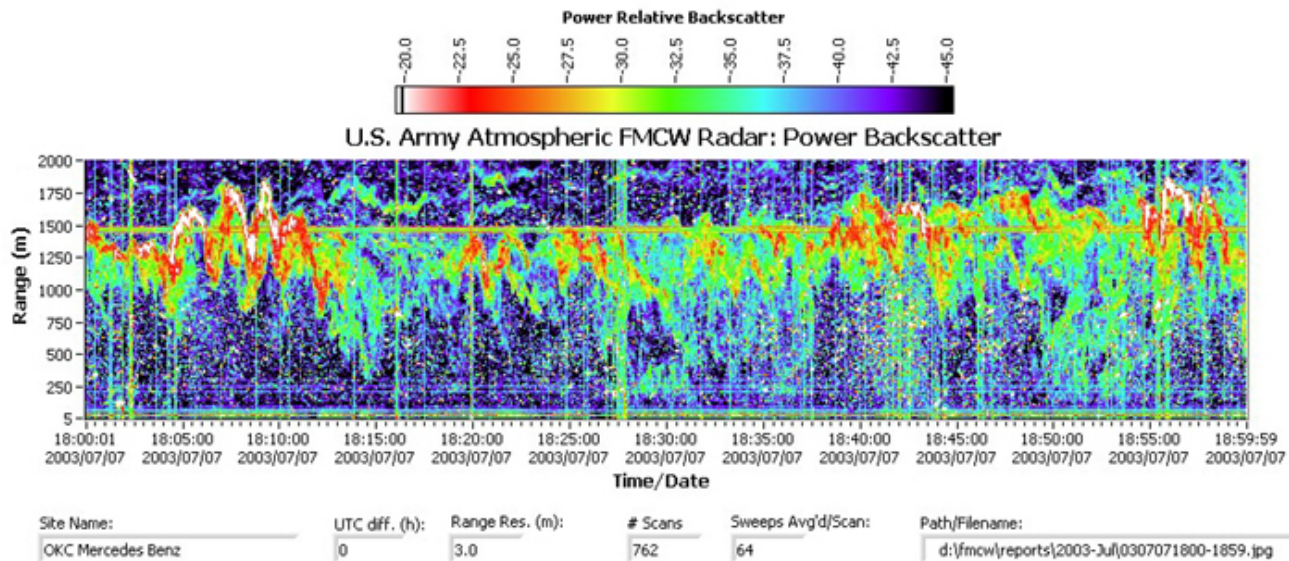


Figure 2 – Vertical profile of (relative) C_n^2 measured by the DPG FM/CW radar on 7 July 2003 from 1800 to 1900 UTC. The top of the convective boundary layer is indicated by stronger backscatter signals as indicated by the yellow, red, and white colors. The abscissa indicates height above ground level (AGL). The point targets, found predominately in the convective boundary layer, are most likely caused by insects. The continuous horizontal lines are from transmitter power supply noise. The intermittent vertical streaks are receiver saturation due to large targets (birds or airplanes) flying through the main beam.

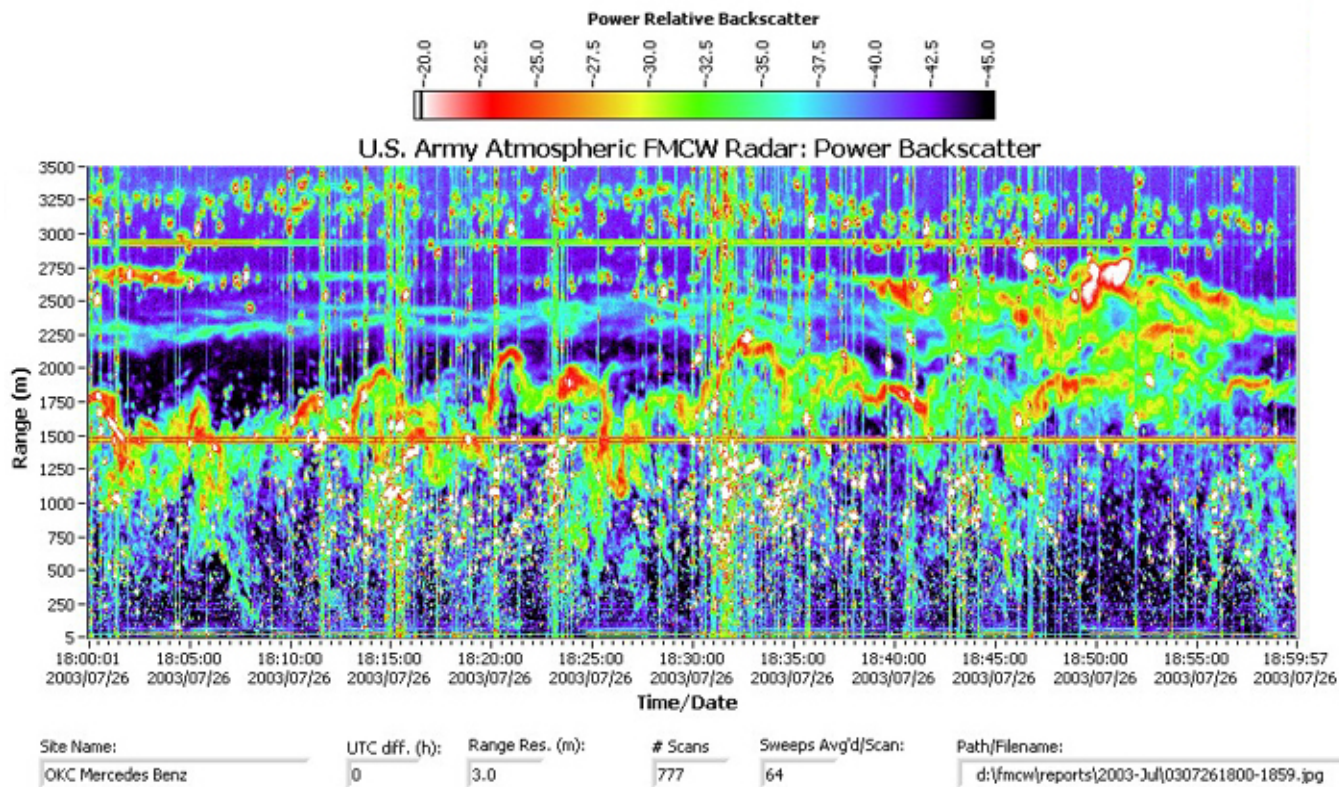


Figure 4 – Vertical profile of (relative) C_n^2 measured by the DPG FM/CW radar on 26 July 2003 from 1800 to 1900 UTC. The convective boundary layer is much higher and has a lower plume development rate than shown in Figure 2. The continuous horizontal lines are from transmitter power supply noise. The intermittent vertical streaks are receiver saturation due to large targets (birds or airplanes) flying through the main beam.

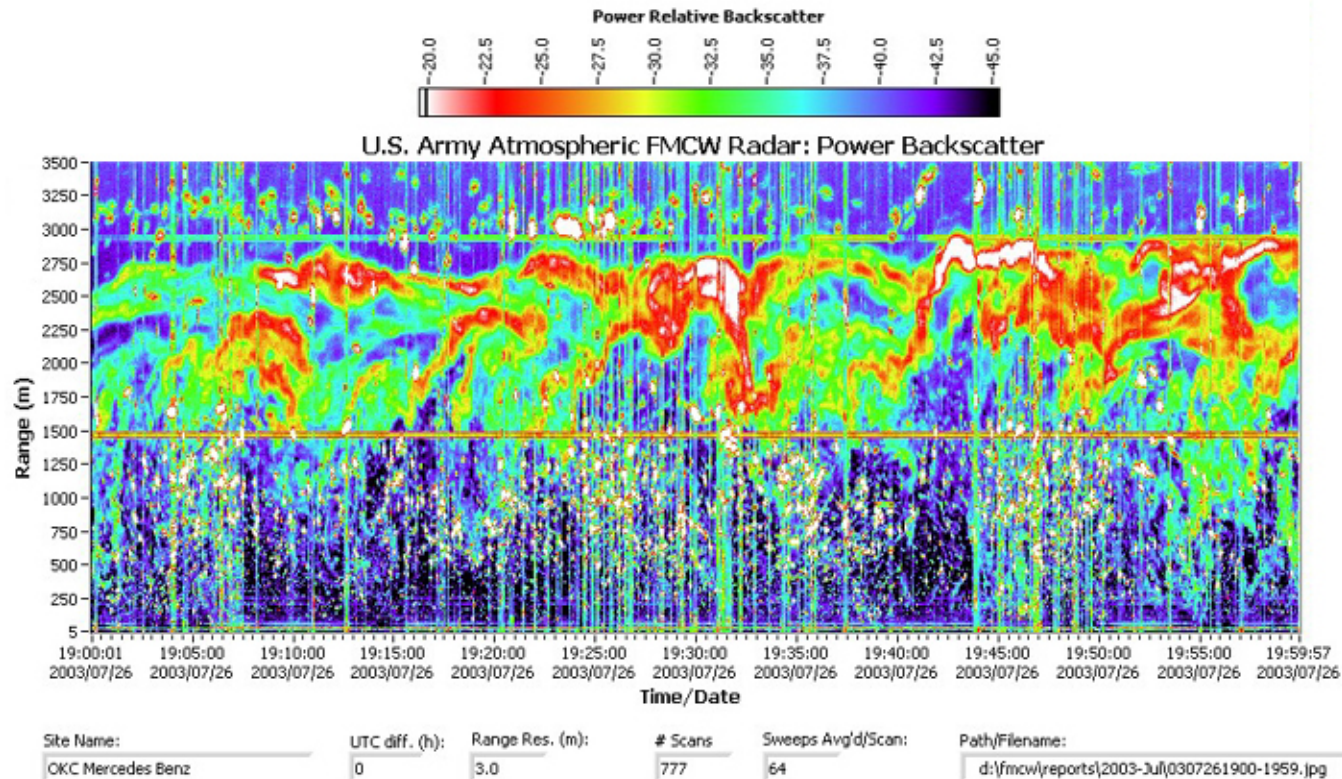


Figure 5 – Vertical profile of (relative) C_n^2 measured by the DPG FM/CW radar on 26 July 2003 from 1900 to 2000 UTC. The top of the boundary layer has become quite turbulent and has risen to an altitude of nearly 3000 m AGL. The vertical lines are radar noise and the horizontal lines at 1450 m and 2850 m are artifacts of the radar transmitter.

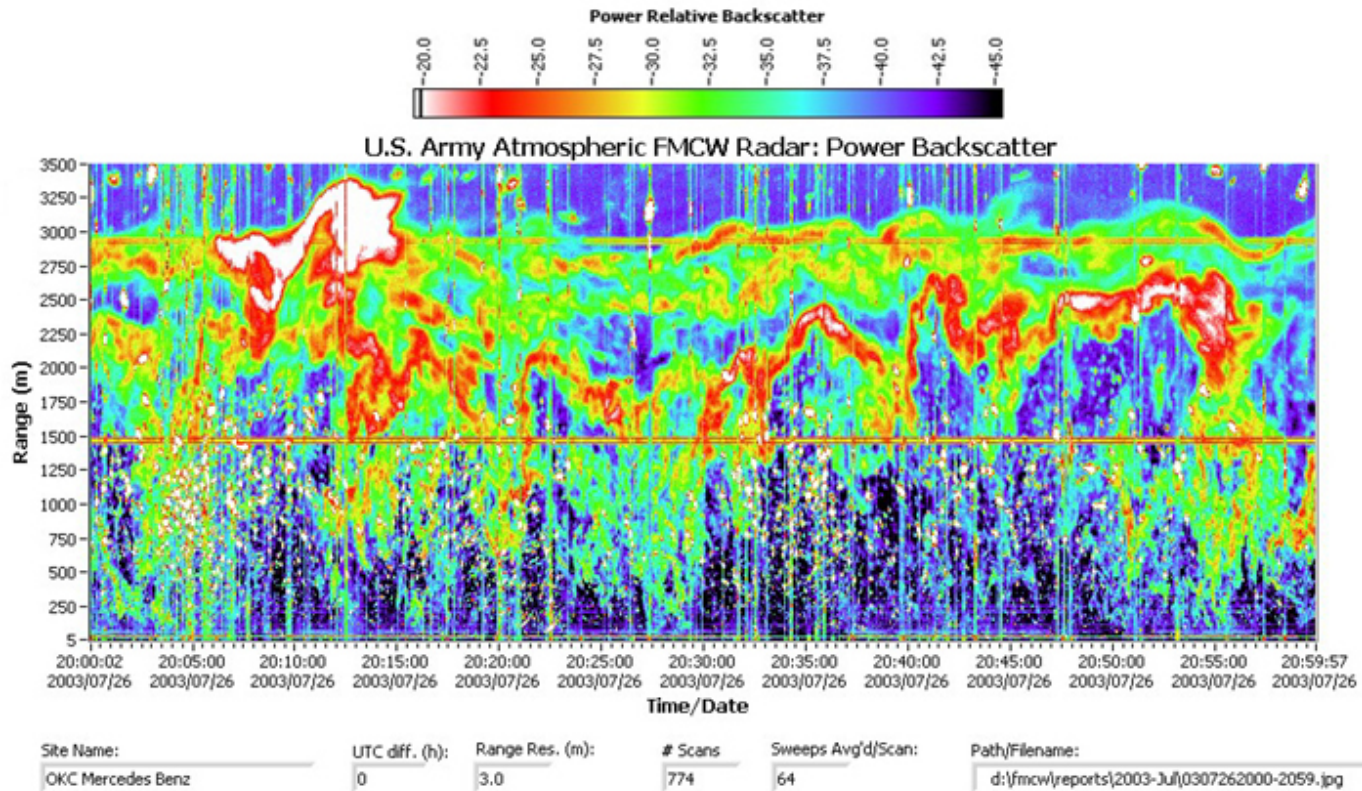


Figure 6 – Vertical profile of (relative) C_n^2 measured by the DPG FM/CW radar on 26 July 2003 from 2000 to 2100 UTC. The “super plume” (at 2010 UTC) is indicated by the strong radar signal extending to a height of nearly 3500 m AGL. Ten minutes following the super plume, the boundary layer falls to a height of approximately 1000 m (at 2020 UTC). The continuous horizontal lines are from transmitter power supply noise. The intermittent vertical streaks are receiver saturation due to large targets (birds or airplanes) flying through the main beam.

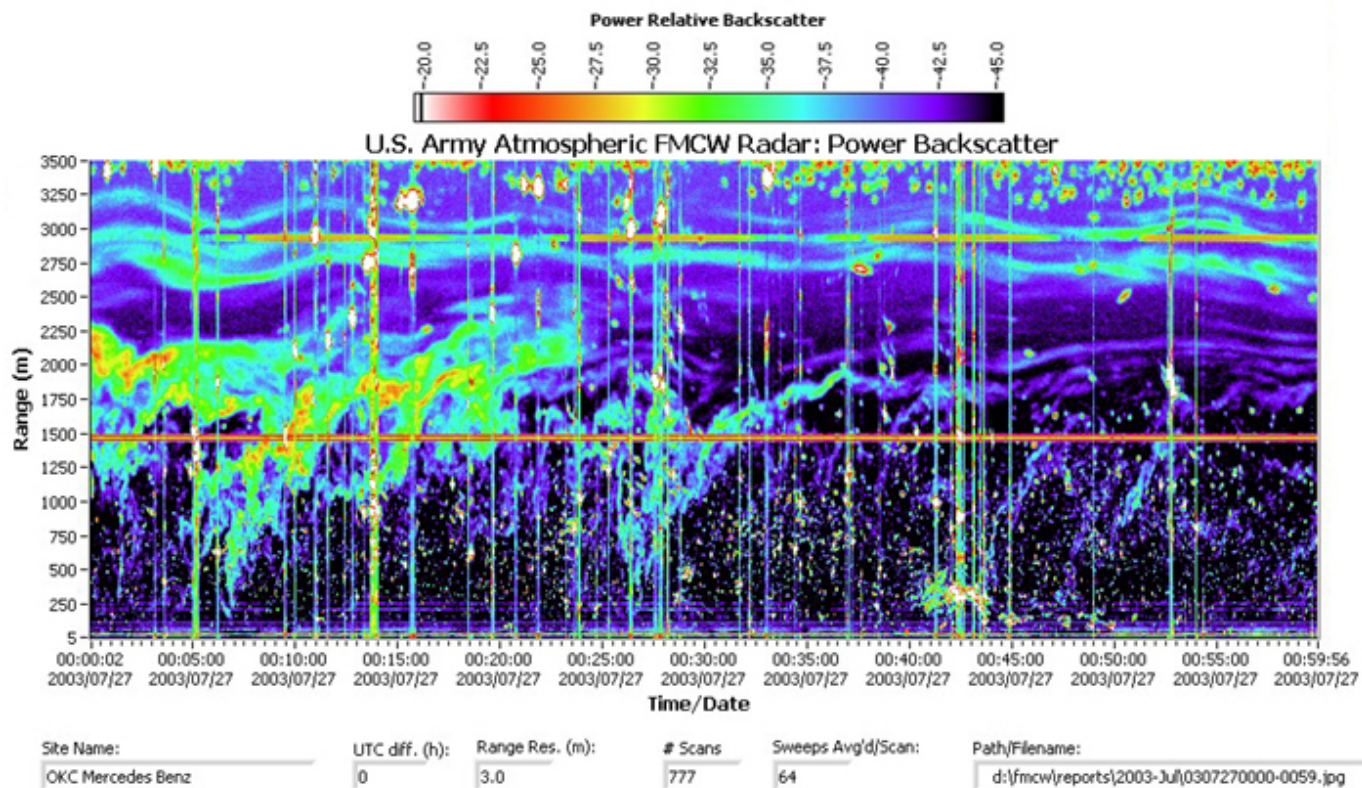


Figure 7 – Vertical profile of (relative) C_n^2 measured by the DPG FM/CW radar on 27 July 2003 from 0000 to 0100 UTC. The demise of the convective boundary layer can be seen by the dramatic decrease in C_n^2 after 0023 UTC. The point targets, most likely caused by insects, remain located at altitudes below the height of the top of the daytime convective boundary layer. The continuous horizontal lines are from transmitter power supply noise. The intermittent vertical streaks are receiver saturation due to large targets (birds or airplanes) flying through the main beam.